ORIGINAL RESEARCH ARTICLE

An investigation on 45S5 nanobioactive glass using FTIR and Raman spectroscopy

Sharda Sundaram Sanjay[1], Pratibha Yadav[1], Nidhi Asthana[2], Mrigank Mauli Dwivedi[2], Kamlesh Pandey[2,*]

[1] *Department of Chemistry, Ewing Christian College, University of Allahabad Allahabad, Uttar Pradesh 211002, India*

[2] *National Center of Experimental Mineralogy and Petrology, University of Allahabad Allahabad, Uttar Pradesh 211002, India*

* Corresponding author: Kamlesh Pandey, kamleshpandey@allduniv.ac.in

ABSTRACT

Bioactive materials are those that cause a number of interactions at the biomaterial-living tissue inter-face that result in the evolution of a mechanically strong association between them. For this reason, an implantable material's bioactive behavior is highly advantageous. Silicate glasses are encouraged to be used as bioactive glasses due to their great biocompatibility and beneficial biological effects. The sol-gel method is the most effective for preparing silicate glasses because it increases the material's bioactivity by creating pores. Glass densities are altered by the internal network connectivity between network formers and network modifiers. The increase in the composition of alkali or alkaline oxides reduces the number of bridging oxygens and increases the number of non-bridging oxygens by retaining the overall charge neutrality between the alkali or alkaline cation and oxygen anion. Higher drying temperatures increase pore densities, while the melt-quenching approach encourages the creation of higher density glasses. Band assignments for the BAG structure can be explained in detail using Fourier Transform Infrared (FTIR) and Raman spectroscopic investigations. Raman spectroscopy makes it simple to measure the concentration of the non-bridging oxygens in the silica matrix.

Keywords: bioactive glass (BAG); FT-IR; Raman spectra; melt-quench; EPMA

1. Introduction

Bioactive materials are becoming an essential component of everyday life. These materials are in between inert and resorbable materials. Bio active materials have the ability to form natural bonds with living tissue[1,2]. During the 1970, this new class of materials, i.e., bioactive glass (BAG), gained attention[3–7]. The first bioactive glass (Bioglass 45S5 with compositions of 45 wt% SiO_2, 24.4 wt% CaO, 24.5 wt% Na_2O, and 6 wt% P_2O_5) was developed and studied by Jones[8] and Hench[9]. BAG is mostly used for biomedical applications and consists of a silicate network incorporating sodium, calcium, and phosphorus in different relative proportions. It exhibits high bioactivity and may attach to soft tissues. Recently, bioactive glass nanoparticles doped with antimicrobial agents such as silver, zinc, and magnesium ions have been widely developed for medical applications. The bioactive glass nanoparticles in a polymeric composite system enable us to develop potential materials for orthopedic applications to avoid health risks[10].

To study the structural changes during the synthesis of BAG, Zachariasen[11] observed that the silicate crystals had a three-

dimensional network structure, which allowed them to easily form glasses upon melting and cooling. It is necessary to keep the cations as far apart as possible and to ensure that each oxygen ion is linked to no more than two cations. Failure to do so would prevent linkage distortion from producing a random network topology. In order to avoid an inflexible octahedral or cubic unit, the coordination number of the oxygen ions surrounding the glass-forming cation must be modest, four or less. With SiO_2, SiO_4^{2-} tetrahedra connected at the corners will form a glass on the basis of the radius ratio. According to Smekal[12], a material's bonding needs to be mixed rather than entirely ionic or totally covalent in order to obtain glass. The covalent bonds have stern bond angles and are strongly oriented. Therefore, a random network structure, which is characteristic of glass, cannot be produced by purely covalent bonding. Ionic bonds, on the other hand, are non-directional and unable to form networks. Thus, a glass needs to have a mixed-character binding[13]. SiO_4 tetrahedra are the basic building blocks of silicate glasses, which are materials that lack long-range order and crystallinity. The SiO_4 tetrahedra can form different types of rings, such as 3-, 4-, or 6-membered rings, depending on the Si–O–Si bond angles and the degree of distortion.

Some examples of how SiO_4 tetrahedra contribute to directional characteristics in the glass network are:

In pure silica glass, the SiO_4 tetrahedra form a random network of mostly 6-membered rings, which have an average Si–O–Si bond angle of 144°. This angle is close to the ideal tetrahedral angle of 109.5°, which minimizes the strain and energy of the network. The 6-membered rings also have a high degree of rotational symmetry, which makes the glass isotropic and transparent.

In soda-lime-silica glass, the addition of sodium and calcium oxides as network modifiers reduces the amount of SiO_4 tetrahedra and introduces non-bridging oxygens (NBOs) in the network. The NBOs break the symmetry of the rings and create more 3- and 4-membered rings, which have smaller and more distorted Si–O–Si bond angles. These rings increase the directionality of the network.

In phosphate glasses, which are a type of bioactive glass that can bond with living tissues, the addition of phosphorus pentoxide as a network former creates a composite structure of separate SiO_4 and PO_4 domains. The PO_4 tetrahedra have a higher charge than the SiO_4 tetrahedra, which makes them more prone to dissolution and precipitation in simulated body fluid. The PO_4 domains also have different ring sizes and shapes than the SiO_4 domains, which create a heterogeneous and adaptable network that can respond to different biological conditions.

Based on the cation's electronegativity, the oxides used in the present study are categorised into two distinct groups. The cation's electronegativity serves as a gauge for the ionic character of the connection because the anion is always oxygen; a lower ionic character is indicated by a higher electronegativity.

(i) Group I cations form bonds with oxygen that have an ionic character larger than fifty percent. They ought to form glass on their own and be network formers. We refer to them as "network formers".
(ii) Group II cations are marginally less electronegative. They can substitute for some of the cations in Group I, but they cannot make glass on their own. We refer to them as intermediates.

We produced a nano bioactive glass (NBAG) using the sol-gel process and melt quench techniques based on an appraisal of the literature. The precursors TEOS, $NaNO_3$, $CaCl_2$, and P_2O_5 are gradually added in four stages of the sol-gel process. According to Albert-Mercier et al.[14] and Deshmukh et al.[15] the network condenses by adding P_2O_5 to the glasses. An increase in P_2O_5 increases the polymerization of the silicate network by increasing the connectivity of the silicate network. P_2O_5 increases the amount of orthophosphate groups in the glass structure, which are the precursors of phosphate compounds that precipitate on the glass surface. The compound, such as hydroxyapatite, forms a strong bond with the bone tissue and enhances the bioactivity of the glass. P_2O_5 coexists with other network former SiO_2 in separate domains within the glass, which creates a composite structure that allows for both dissolution and precipitation processes to occur

simultaneously.

The Na_2O content in BAG affects the glass transition temperature (T_g). An increase in Na_2O content decreases T_g. The sintering process of glasses depends on properties like the glass transition temperature and the peak crystallization temperature. A large difference between T_g and crystalline temperature (T_c) is required to ensure that the glass sinters without crystallizing. Crystallization of a BAG inhibits its bioactive properties in the presence of crystalline phases[16–18].

In this process, the hydrolysis and poly-condensation of precursors result in the formation of the disordered glass network, and the addition of sodium and calcium salts triggers the gelation of the sol. There is limited literature regarding temperature-dependent FTIR studies conducted at different stages for bioactive glasses. The comprehensive data in this work provides a panoramic view of the intermediate constituents and their influence on bonding during the process, which is therefore crucial. In the present study, we report the changes in structural behaviour during the process of gelification as well as the melt-quench method by FTIR, laser Raman technique, and electron-probe micro analyser.

2. Experimental

We have synthesised the following five bioactive glass compositions using both melt quench and sol gel synthesis method:

(i) 70% SiO_2-30% CaO (BAG-1)
(ii) 45% SiO_2-24.5% Na_2O-24.5% CaO-6% P_2O_5 (45S5) (BAG-2)
(iii) 53% SiO_2-23% Na_2O-20% CaO-4% P_2O_5 (BAG-3)
(iv) 58% SiO_2-33% CaO-9% P_2O_5 (BAG-4)
(v) 53% SiO_2-6% Na_2O-20% CaO-12% K_2O-5% MgO-4% P_2O_5(BAG-5)

In the present study the composition 45S5 was considered. In the melt-quenching method, glass is obtained by mixing, homogenizing, calcining, and fusing glass precursors such as oxides or carbonates at 1500 ℃. The starting materials were SiO_2 (99%, RENKEM, India), $CaCO_3$ (98%, RENKEM, India, Na_2CO_3 (98%, RENKEM, India) and P_2O_5 (99.9%, Glaxo, India). Glass batches of 5 g were prepared by melt-quenching. For that, the starting materials were mixed homogeneously in acetone as mixing media for 2 h and then dried at 110 ℃. The mixtures were melted in a platinum crucible in a two-step process. Firstly, they were heated up to 1500 ℃ with a heating rate of 10 ℃/min, with a holding step for 1 h. Finally, the melted compositions were quenched in cold water (0 ℃). This procedure was repeated twice to ensure homogeneity of the specimens. Afterwards, the glasses were ground in an agate mortar and pestle.

While synthesing BAG through sol-gel technique, the composition by weight percent was maintained as 45 SiO_2 - 24.5 Na_2O - 24.5 CaO - 6 P_2O_5. Tetraethyl-orthosilicate (TEOS), $Si(OC_2H_5)_4$, supplied by ACROS-Organics, was used as the Si network precursor, while sodium nitrite $NaNO_3$ and calcium nitrate/chloride $Ca(NO_3)_2$ (98%, Lobachem, India),were selected as Na and Ca network modifiers respectively. Two separate solutions were prepared. First contains the network precursor and other network modifier. In network precursor TEOS (9 mL ∼ 4.5 g SiO_2) was hydrolysed in ethanol and acidified with acetic acid in the 1:4:1 ratio under the magnetic stirring for 120 min, until a transparent sol was formed. The other solution of sodium nitrate and calcium nitrate (equivalent to 1.22 g of each Na_2O and CaO) were dissolved in 10 mL double distilled water for one hours. Afterward both solutions were mixed in TEOS sol separately. Finally, P_2O_5 powder (300 mg) was dissolved in same sol and the final solution was stirred for 24 h at room temperature. This solution was stored at 70 ℃ for 120 h to get the gel. To promote a relatively fast sol-gel transition, the gel was kept at 200 ℃ for 24 h, after this the xerogel was crushed with agate pestle and mortar into a fine powder and then calcined at 350 ℃ and 700 ℃ for 10–15 h. The FTIR spectra (in the wave

number range 1200–700 cm^{-1}) of sol with different time span reaction (0–3000 s) was also recorded.

The sintered specimen powder was characterized by ATR-FTIR (Bruker-Alpha, Germany) in the wavenumber 4000 cm^{-1} to 400 cm^{-1}, Raman spectra were collected with Uniram confocal Raman spectrophotometer with laser sources at 785 nm with variable power in the spectral range (100–2000 cm^{-1}). The surface morphology and compositional analysis of the melt quench synthesised BAG was analysed by JEOL-JXA-8100, Electron probe micro-analyser. For this the sample was mounted on epoxy resin and then grinded and polished to a very smooth surface and then coated with 20–30 nm layer of carbon for making the surface conducting.

3. Results and discussion

The FTIR spectra of bioactive glass in range 4000 cm^{-1}–2500 cm^{-1} and 1500 cm^{-1}–600 cm^{-1} at different stages is shown in **Figure 1**. The **Figure 1A**, shows a broad peak present around 3300 cm^{-1} assigned as –OH stretching in the FTIR range of 2000 cm^{-1}–4000 cm^{-1}, in sol-gel prepared BAG 45S5. When gel is dried at 200 °C, then this peak completely disappeared. In **Figure 1B** different FTIR spectra of sol gel prepared BAG-2 are recorded at various stage of gelification. The comparative study of these spectra (in range 1500–600 cm^{-1}) clearly indicates the chemical changes and continuous decrease in their intensity up to 150 h at 70 °C (temperature of gelification), a new peak pattern at same temperature indicates the intermediate phase formation in between 150–170 h. At 200 °C (gel drying temperature), this peaks pattern almost disappeared. **Figure 1C**, explains the effect of Na$_2$O, CaO and P$_2$O$_5$, here, it is clear that peaks at 783 cm^{-1} and 1166 cm^{-1} of hydrolysed TEOS are completely vanished when NaNO$_3$ is mixed in the solution. Similar effect of CaNO$_3$ is also observed. The effect of P$_2$O$_5$ in the matrix, reduces the broadness of peak around 1400 cm^{-1}. This effect is also observed in the **Figure 1D**, where glass sample without P$_2$O$_5$ have no peak around the 1400 cm^{-1} region.
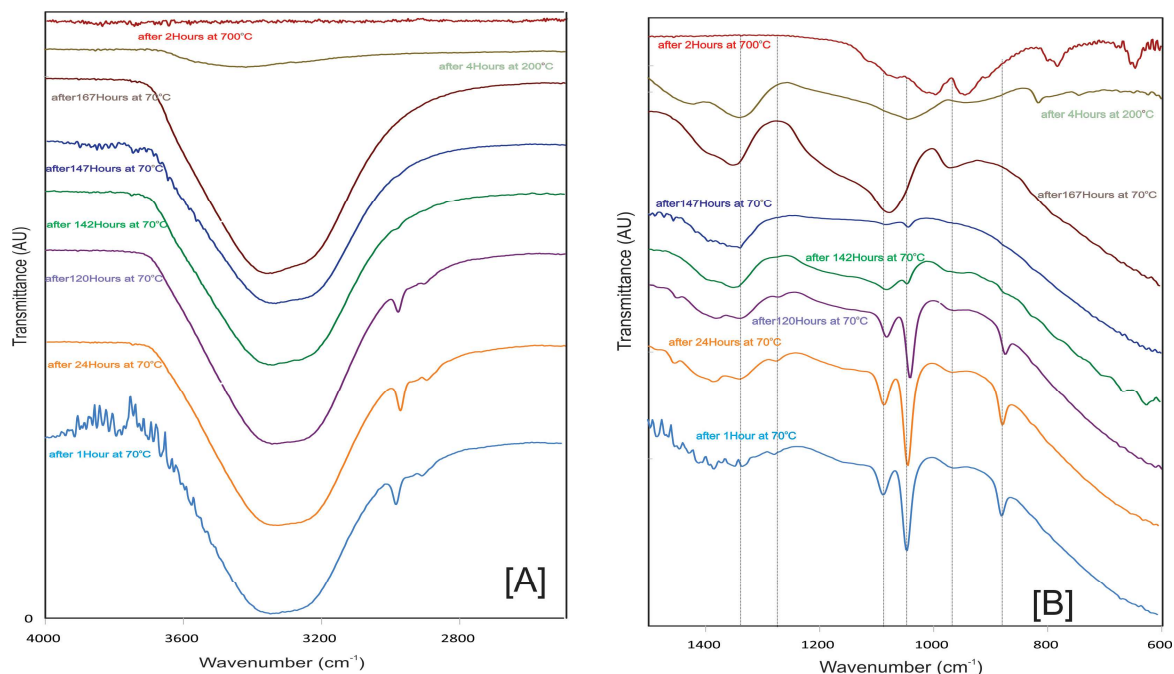
Figure 1. (*Continued*).
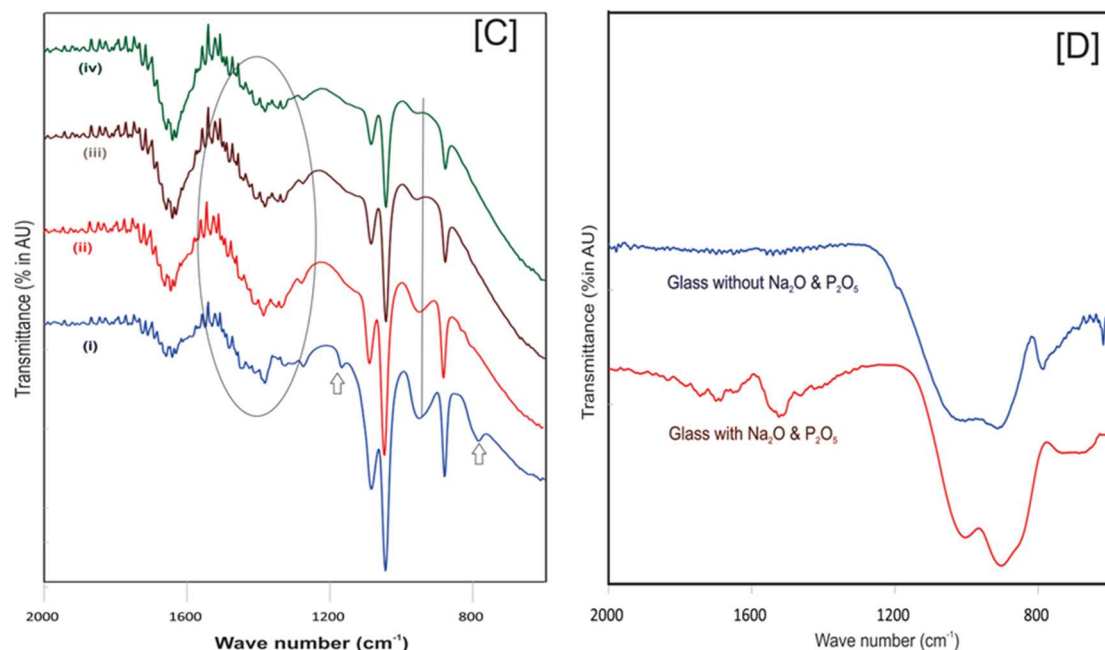
Figure 1. Different stages of FT-IR spectra of bioactive glass **(A)** in the region (4000–2500 cm^{-1}); and **(B)** in the region (1500–600 cm^{-1}); **(C)** effect of different constituents (i) sodium nitrate (ii) calcium nitrate (iii) P$_2$O$_5$; **(D)** FTIR spectra of melt quench glasses with and without Na$_2$O and P$_2$O$_5$.

In **Figure 2** the rapid three dimensional time span reaction (with time in seconds) is presented from starting material to partial stabilisation of reaction process of BAG formation.

The other important features in the gelification process with small interval of time (**Figure 2**) is as follows The FTIR spectrum at 30 s. in the homogeneous solution of TEOS, H$_2$O and acetic acid show strong bands at 1110 cm^{-1}, 1070 cm^{-1}, and 955 cm^{-1} and medium and small bands at 1165 cm^{-1} and 809 cm^{-1}, all attributed due to TEOS. The peak at 1052 cm^{-1} and 880 cm^{-1} are due to ethanol.
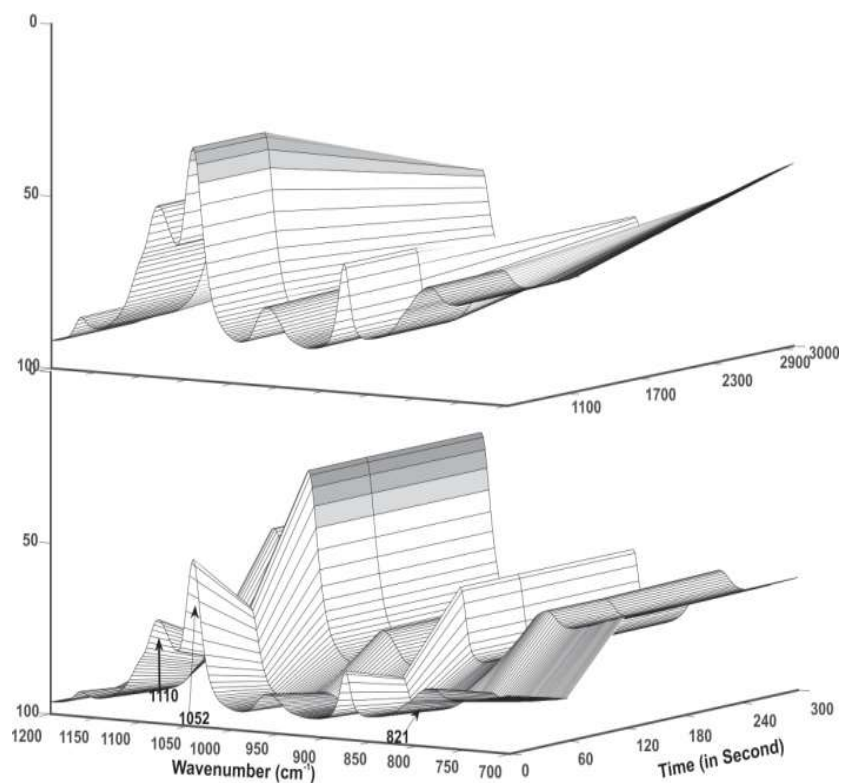
Figure 2. FT-IR spectra of BAG formation starting from hydrolysis of TEOS with time 0–3000 s in 1200 cm^{-1}–600 cm^{-1} range.

5

With the increasing time, the intensity of the of the main peaks of TEOS tries to reduce their intensity and the intensity of ethanol peaks 1052 cm^{-1} and 880 cm^{-1} increases and after 500 s, it becomes almost constant.

It is also observed that the absorbance values of Si–O–C stretching bands of TEOS at 1105 cm^{-1} and 1080 cm^{-1} show a sudden enhancement during the time span 200 s. this shift is possibly due to the alteration of the dipole moment of the Si–O–C vibrations as a result of the reaction of acetic acid during hydrolysis. After 400 s. most of the TEOS peak disappeared, but the intensity of the peak 950 (Si–OH, silanol group) increases. Peaks at 805 cm^{-1} and 1165 cm^{-1} (i.e., Si–O–Si sym. and LO components respectively) appears in later stage due to the formation of SiO_4 network formation of SiO_2. In the initial stage some peaks tries to overlap/superimpose.

A comparative FT-IR spectra of liquid TEOS, hydrolysed TEOS and final Silica powder are given in **Figure 3**. The Raman spectra of TEOS hydrolysis process with sol-gel BAG-2 and melt—quench synthesised BAG-2 is shown in **Figure 4**.
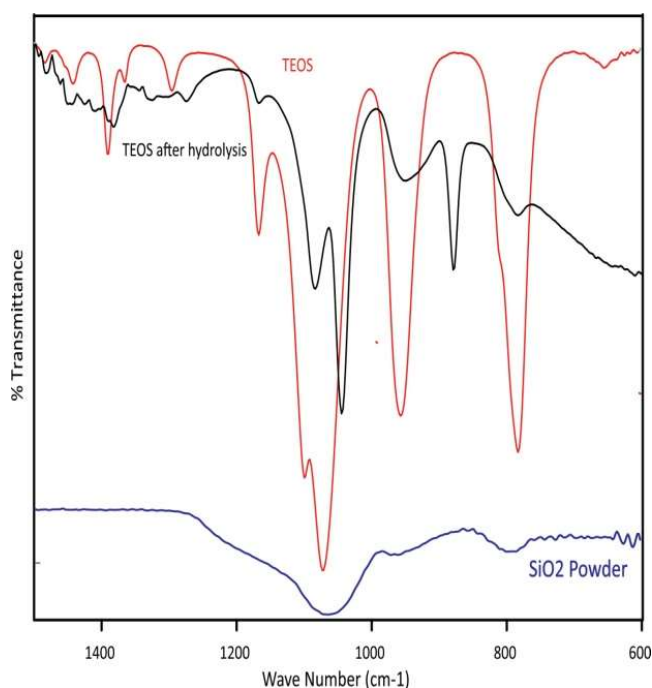
Figure 3. FT-IR spectra of TEOS, hydrolysed TEOS and SiO_2 powder in 1500 cm^{-1}–600 cm^{-1} range.

Figure 4. Raman spectra of BAG **(A)** at different stages of temperature; **(B)** BAG and SiO_2 powder by sol gel; **(C)** BAG by melt quench with compositional image of BAG by EPMA.

On the basis of these stepwise interaction's studies (mainly peaks of the FT-IR and Raman spectra), following reaction mechanism for the final glass formation can be deduced[19–22]. The logical explanation for each reaction mechanism is given along with each equation:

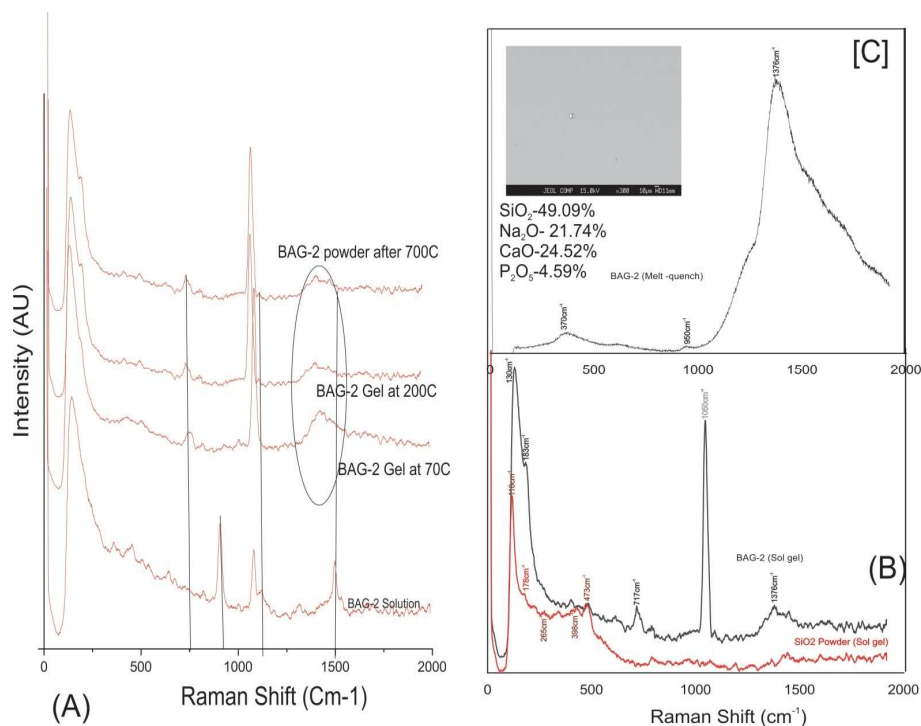- Disappearance of red shift of intense C–H rocking peak at 959 cm^{-1} due to CH$_3$ of TEOS to a less intense broad peak at 951 cm^{-1} indicated the formation of Si–OH group (Equation (1)).

$$C_2H_5O-\underset{\underset{O-C_2H_5}{|}}{\overset{\overset{O-C_2H_5}{|}}{Si}}-OCH_2 \;+\; H_2O \;\rightleftharpoons\; C_2H_5O-\underset{\underset{O\;\;C_2H_5}{|}}{\overset{\overset{O-C_2H_5}{|}}{Si}}-OH \;+\; C_2H_5OH \tag{1}$$
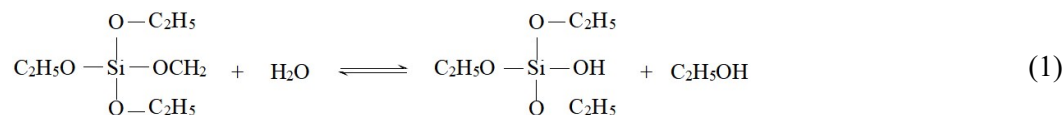
- Si–O–Si bend frequency mode at 782 cm^{-1} is revealing hydrolysis. This is also confirmed in Raman spectral peak at 1050 cm^{-1}, which confirms the formation of siloxane network on condensation (Equation (2)).

$$C_2H_5O-\underset{\underset{O-C_2H_5}{|}}{\overset{\overset{O-C_2H_5}{|}}{Si}}-O[H \;+\; HO]-\underset{\underset{O\_C_2H_5}{|}}{\overset{\overset{O-C_2H_5}{|}}{Si}}-OC_2H_5 \;\rightleftharpoons\; C_2H_5O-\underset{\underset{O\;\;C_2H_5}{|}}{\overset{\overset{O-C_2H_5}{|}}{Si}}-O-\underset{\underset{O-C_2H_5}{|}}{\overset{\overset{O-C_2H_5}{|}}{Si}}-OC_2H_5 \;+\; H_2O \tag{2}$$
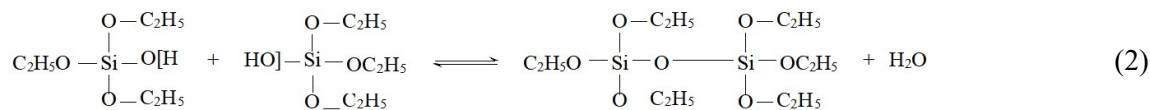
- Red shift of the peak at 1042 cm^{-1} due to stretching and bending vibrations shows the change in dipole moment of Si–O–C fragment. In Raman spectra peak at 880 cm^{-1} is of C–C–O stretching vibrations of ethanol which disappears at higher temperature indicating the evaporation of ethanol (Equation (3)).

$$C_2H_5O-\underset{\underset{O-C_2H_5}{|}}{\overset{\overset{O-C_2H_5}{|}}{Si}}-O[H \;+\; C_2H_5O]-\underset{\underset{O\_C_2H_5}{|}}{\overset{\overset{O-C_2H_5}{|}}{Si}}-OC_2H_5 \;\rightleftharpoons\; C_2H_5O-\underset{\underset{O\;\;C_2H_5}{|}}{\overset{\overset{O-C_2H_5}{|}}{Si}}-O-\underset{\underset{O\;\;C_2H_5}{|}}{\overset{\overset{O-C_2H_5}{|}}{Si}}-OC_2H_5 \;+\; C_2H_5\,OH \tag{3}$$

- Peak at 1081 cm^{-1} C–O asymmetric stretch in ethanol (Equations (1) and (3)).
- Decreasing intensity at 1167 cm^{-1} shows the disappearance of –OC$_2$H$_5$ group due to repeated hydrolysis and condensation giving following product (Equation (4)).

$$-\!\!-O-\underset{\underset{OH}{|}}{\overset{\overset{C_2H_5}{|}}{Si}}-O-\underset{\underset{OH}{|}}{\overset{\overset{C_2H_5}{|}}{Si}}-O-\underset{\underset{OH}{|}}{\overset{\overset{C_2H_5}{|}}{Si}}-O-\underset{\underset{OH}{|}}{\overset{\overset{C_2H_5}{|}}{Si}}-OH \qquad (4)$$

- The incorporation of Na and Ca in the silica lattice is observed in their hydrolysed form at 1657 cm^{-1} and 1641 cm^{-1} respectively (Equations (5) and (6)).

$$-\!\!-O-\underset{\underset{OH}{|}}{\overset{\overset{C_2H_5}{|}}{Si}}-O-\underset{\underset{OH}{|}}{\overset{\overset{C_2H_5}{|}}{Si}}-O-\underset{\underset{OH}{|}}{\overset{\overset{C_2H_5}{|}}{Si}}-O-\underset{\underset{OH}{|}}{\overset{\overset{C_2H_5}{|}}{Si}}-OH \ +\ NaNO_3 \ \rightleftharpoons\ -\!\!-O-\underset{\underset{ONa}{|}}{\overset{\overset{C_2H_5}{|}}{Si}}-O-\underset{\underset{ONa}{|}}{\overset{\overset{C_2H_5}{|}}{Si}}-O-\underset{\underset{ONa}{|}}{\overset{\overset{C_2H_5}{|}}{Si}}-O-\underset{\underset{ONa}{|}}{\overset{\overset{C_2H_5}{|}}{Si}}-ONa \ +\ HNO_3 \qquad (5)$$

$$\text{(structure)}\ +\ Ca(NO_3)_2 \ \rightleftharpoons\ \text{(structure)}\ +\ CaSiO_3 + NaNO_3 \qquad (6)$$

- Intense peak at 878 cm^{-1} indicates the formation of SiO$_4$ network. A characteristic vibrational mode of $[P_2O_7]^{4-}$ (pyrophosphate) were also observed at 878 cm^{-1} which persist even at 700 °C with a little red shift at 784 cm^{-1} indicating the presence of bridge P–O–P within the silaxanol lattice (Equation (7)).

$$\text{(structure)}\ +\ P_2O_5 \ \xrightarrow{\text{dehydrating agent}}\ \text{SiO}_2 \text{ gel network} \qquad (7)$$

SiO$_2$ gel network

The Raman spectra (**Figure 4**) also reveals the fact:

(i)   The sharp peak at 1500 cm^{-1} is due to –CH$_2$ bending vibrations and is also red shifted and become broad after gelification and the broadness reduces after drying the sample.

(ii) It is also important to observe the appearance of some new peaks during the process of gelification. At 750 cm^{-1} the peak is due to P–O–P bridging oxygen (Equation (6)) There is a clear increase in the intensity of 1050 cm^{-1} peak is due to dominant role of phosphorus in gel matrix (Equation (4))[23–26].

(iii) Another evidence of the existence of the phosphorus in the form of P = O (1376 cm^{-1}—Raman peak) of P$_2$O$_5$. It may be due to the formation of pπ–dπ dative bond (**Figure 5**) along with P–O σ bond, introducing double bond character, which in turn strengthen the P–O (NBO) bonds. This P exist up to 800 °C and finally forming pyro-phosphate. On comparing **Figure 4B,C**, clearly indicating that the pyro-phosphate does not exist in the melt-quench BAG π structure, but the peak at 1050 cm^{-1} red shifted with very small intensity at 950 cm^{-1}, which is the indication of the formation of o-phosphate (NBO) in the matrix. This o-phosphate is formed because there is rapid increase and quenching of the temperature during the glass formation.
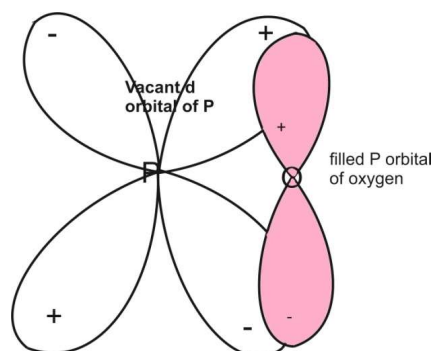
Figure 5. Showing pπ–dπ overlap between O and P orbital.

This result is also confirmed in 'Electron Probe Micro Analysis' (EPMA) of melt quench BAG-2 powder in the inset of **Figure 4** the presence of P_2O_5 (estimated quantity in final glass 4.8%) is more or less same amount as in the host matrix.

4. Conclusion

A study confirms that SiO_4 tetrahedra provide some directional characteristics to form a sort of network, while sodium and calcium introduc randomness in the structure. P_2O_5 helps in the reinforcement of stable bonds to form an efficient bioactive glass. A systematic mechanism of the glass formation is deduced with the help of IR and Raman spectra; moreover, EPMA confirms the presence of P–O in the final glass matrix even at elevated temperatures.

Author contributions

Conceptualization, KP and SSS; methodology, KP; validation, KP, MMD and SSS; formal analysis, KP, NA and PY; investigation, KP and PY; resources, KP and PY; writing—original draft preparation, KP, NA and SSS; writing—review and editing, KP and MMD; visualization, KP and MMD; supervision, KP. All authors have read and agreed to the published version of the manuscript.

Acknowledgments

Conflict of interest

The authors declare no conflict of interest.

References

1. Silva MJ, Alves W, Graeff CFO, et al. Modified synthesis and physicochemical characterization of a bioglass-based composite for guided bone regeneration. *The Scientific World Journal* 2021; 2021: 1–9. doi: 10.1155/2021/4295433

2. Chapekar MS. Tissue engineering: Challenges and opportunities. *Journal of Biomedical Materials Research* 2000; 53(6): 617–620. doi: 10.1002/1097-4636(2000)53: 6<617:: aid-jbm1>3.0.co,2-c

3. Cao W, Hench LL. Bioactive materials. *Ceramics International* 1996; 22(6): 493–507. doi: 10.1016/0272-8842(95)00126-3

4. Hench LL, Splinter RJ, Allen WC, et al. Bonding mechanisms at the interface of ceramic prosthetic materials. *Journal of Biomedical Materials Research* 1971; 5(6): 117–141. doi: 10.1002/jbm.820050611

5. Kokubo T. Bioactive glass ceramics: Properties and applications. *Biomaterials* 1991; 12(2): 155–163. doi: 10.1016/0142-9612(91)90194-f

6. Adams LA, Essien ER, Adesalu AT, et al. Bioactive glass 45S5 from diatom biosilica. *Journal of Science: Advanced Materials and Devices* 2017; 2(4): 476–482. doi: 10.1016/j.jsamd.2017.09.002

7. Hench LL, Polak JM. Third-generation biomedical materials. *Science* 2002; 295(5557): 1014–1017. doi:

10.1126/science.1067404

8. Jones JR. Review of bioactive glass: From hench to hybrids. *Acta Biomaterialia* 2013; 9(1): 4457–4486. doi: 10.1016/j.actbio.2012.08.023

9. Hench LL. The story of Bioglass®. *Journal of Materials Science: Materials in Medicine* 2006; 17(11): 967–978. doi: 10.1007/s10856-006-0432-z

10. Sepulveda P, Jones JR, Hench LL. Characterization of melt-derived 45S5 and sol-gel–derived 58S bioactive glasses. *Journal of Biomedical Materials Research* 2001; 58(6): 734–740. doi: 10.1002/jbm.10026

11. Zachariasen WH. The atomic arrangement in glass. *Journal of the American Chemical Society* 1932; 54(10): 3841–3851. doi: 10.1021/ja01349a006

12. Smekal A. The nature of the mechanical strength of glass. *J. Soc. of Glass Tech* 1936; 20: 432–448.

13. Gibbs GV, Cox DF, Crawford TD, et al. Classification of metal-oxide bonded interactions based on local potential- and kinetic-energy densities. *The Journal of Chemical Physics* 2006; 124(8). doi: 10.1063/1.2161425

14. Albert-Mercier C, Follet C, Pardini A, Revel B. Influence of P_2O_5 content on the structure of SiO_2-Na_2O-CaO-P_2O_5 bioglasses by ^{29}Si and ^{31}P MAS-NMR. *Journal of Non-Crystalline Solids* 2011; 357(24): 3901–3909. doi: 10.1016/j.jnoncrysol.2011.07.042

15. Deshmukh K, Kovářík T, Křenek T, et al. Recent advances and future perspectives of sol–gel derived porous bioactive glasses: A review. *RSC Advances* 2020; 10(56): 33782–33835. doi: 10.1039/d0ra04287k

16. Hannon AC. Basic concepts of network glass structure. In: Richet P, Concradt R, Takada A, Dyon J (editors). *Encyclopedia of Glass Science, Technology, History, and Culture*. John Wiley & Sons; 2021. pp. 129–140. doi: 10.1002/9781118801017.ch2.1

17. Wallace KE, Hill RG, Pembroke JT, et al. Influence of sodium oxide content on bioactive glass properties. *Journal of Materials Science: Materials in Medicine* 1999; 10(12): 697–701. doi: 10.1023/a: 1008910718446

18. Kuzielova E, Palou M, Kozankova J. Crystallization Mechanism and bioactivity of Lithium disilicate glasses in relation to CaO, P_2O_5, CaF_2 addition. *Ceramic Silikaty* 2007; 51(3): 136–141.

19. Boccaccini AR, Blaker JJ. Bioactive composite materials for tissue engineering scaffolds. *Expert Review of Medical Devices* 2005; 2(3): 303–317. doi: 10.1586/17434440.2.3.303

20. Verweij H, Konijnendijk WL. Structural units in K_2O-PbO-SiO_2 glasses by Raman spectroscopy. *Journal of the American Ceramic Society* 1976; 59(11–12): 517–521. doi: 10.1111/j.1151-2916.1976.tb09422.x

21. Vyas VK, Kumar AS, Singh SP, et al. Effect of nickel oxide substitution on bioactivity and mechanical properties of bioactive glass. *Bulletin of Materials Science* 2016; 39(5): 1355–1361. doi: 10.1007/s12034-016-1242-7

22. Ershad M, Ali A, Mehta NS, et al. Mechanical and biological response of (CeO_2 + La_2O_3)-substituted 45S5 bioactive glasses for biomedical application. *Journal of the Australian Ceramic Society* 2020; 56(4): 1243–1252. doi: 10.1007/s41779-020-00471-3

23. Oliveira AAR, Gomide VS, Leite MDF, et al. Effect of polyvinyl alcohol content and after synthesis neutralization on structure, mechanical properties and cytotoxicity of sol-gel derived hybrid foams. *Materials Research* 2009; 12(2): 239–244. doi: 10.1590/s1516-14392009000200021

24. Aina V, Malavasi G, Fiorio Pla A, et al. Zinc-containing bioactive glasses: Surface reactivity and behaviour towards endothelial cells. *Acta Biomaterialia* 2009; 5(4): 1211–1222. doi: 10.1016/j.actbio.2008.10.020

25. Kim IY, Kawachi G, Kikuta K, et al. Preparation of bioactive spherical particles in the CaO–SiO$_2$ system through sol–gel processing under coexistence of poly(ethylene glycol). *Journal of the European Ceramic Society* 2008; 28(8): 1595–1602. doi: 10.1016/j.jeurceramsoc.2007.11.006

26. Mohan Babu M, Syam Prasad P, Hima Bindu S, et al. Investigations on physico-mechanical and spectral studies of Zn^{2+} doped P_2O_5-based bioglass system. *Journal of Composites Science* 2020; 4(3): 129. doi: 10.3390/jcs4030129